Available online at www.sciencedirect.com
SCIENCE DIRECT®
Physica A 325 (2003) 78–91
PHYSICA A
www.elsevier.com/locate/physa

Anomalous interstitial dynamics, Stokes' drift, and current inversion in AC-driven vortex lattices in superconductors with arrays of asymmetric double-well traps

F. Marchesoni[a,b], B.Y. Zhu[a], Franco Nori[a,c,*]

[a] *Frontier Research System, The Institute of Physical and Chemical Research (RIKEN), Wako-shi, Saitama 351-0198, Japan*
[b] *Istituto Nazionale di Fisica della Materia, Universitá di Camerino, I-62032 Camerino, Italy*
[c] *Center for Theoretical Physics, Physics Department, CSCS, The University of Michigan, Ann Arbor, MI 48109-1120, USA*

Received 26 November 2002

Abstract

Using numerical simulations, we study the response, to an AC square-wave Lorentz force, of an assembly of magnetic vortices interacting with a square lattice of double-well asymmetric pinning centers. The collective AC-driven vortex dynamics becomes rectified for drive amplitudes within an optimal rectification window. Here we focus on the dynamics right above the first matching field, where there are slightly more vortices than pinning traps. Remarkably, for low drive amplitudes the excess vortices, i.e., not sitting in the pinning centers, behave either like highly mobile interstitials confined between two adjacent columns of vortices, or like stable discommensurations of single lattice columns. In both cases these excess vortices exhibit a variety of dynamical responses (e.g., current inversion, Stokes' drift) depending on the amplitude of the applied force.

PACS: 05.40.−a; 74.60.Ge

Keywords: Vortex dynamics in superconductors; Ratchets; Vortex pinning; Interstitial dynamics; Discommensurations

* Corresponding author. Laboratory Head, Digital Materials Lab. Frontier Research System, RIKEN, 2-1 Hirosawa, Wako shi, Saitama 351-0198, Japan. Tel.: +81-48-467-9707; fax: +81-48-467-9650.
E-mail address: fnori@riken.jp (F. Nori).

0378-4371/03/$ - see front matter
doi:10.1016/S0378-4371(03)00186-9

1. Introduction

Solid state structures with asymmetric potentials are currently attracting considerable attention [1,2] because they provide novel ways to control the motion of particles in devices. These were initially motivated by work on Brownian motors [3–6] Controlling the motion [7] of magnetic flux quanta in superconductors is of potential application for very sensitive SQUID sensors of magnetic flux [8] and for other applications, including the design of novel magnetic flux pumps, diodes, as well as for focusing and lensing magnetic flux quanta in designated target regions inside a superconducting device [9–15].

Vortex dynamics in asymmetric superconducting devices driven by an external AC force is a very new development [9–15] that promises an unprecedented degree of control of the motion of flux quanta, including easily controllable collective step-motors, magnetic flux concentrators and flux dispersers, vortex brooms, etc.. The combination of a driving force which is periodic in time and a certain degree of spatial asymmetry in the potential energy felt by the movable objects induces a net stationary time-averaged transport of vortices along one direction. This DC rectification of an AC-driven system is known as the ratchet effect [3]. Rectification of AC driven vortex dynamics has been achieved by means of several mechanisms. Three of these are summarized here: (i) Asymmetric *boundaries* [9] that allow freely moving vortices, which are pumped back and forth through channels with suitably corrugated walls, to achieve a net average DC velocity; (ii) Asymmetrically modulated spatial distributions (for distances $\sim\lambda$) of otherwise symmetric pinning centers [10], where a coarse-grained (for distances $\sim\lambda$ or larger) effective ratchet potential is generated by the vortices trapped in the pins, and only the interstitial flow gets rectified. Here λ denotes the length-scale beyond which the vortex-vortex interactions decrease very fast. The length-scale ξ, which is much smaller than λ, denotes the typical vortex core size, which is of the same order of magnitude as the pinning force interaction; (iii) Regular lattices of asymmetric double-well pinning centers [11,12], where rectification occurs at the length scale of the pins ($\sim\xi$ as opposed to the scale of $\sim\lambda$ in Ref. [10]) and acts on the entire vortex array, with no distinction between interstitial and trapped vortices.

Twin boundaries in flux-gradient-driven vortices, as opposed to the current-driven vortices considered by most theoretical studies, can also be used as vortex diodes [13]. All of the above systems are intrinsically two-dimensional, whereas the potential energy considered in Ref. [14] is essentially one-dimensional. Also, all previous proposals are based on spatially-asymmetric substrates. Recently, time-asymmetric driving has been used for samples that have no spatial asymmetry [15].

In the present work we study the interstitial vortex flow appearing in configuration (iii), namely for superconducting samples with a square array of asymmetric double-well pinning centers [11,12]. These type of samples can be produced in the laboratory via controlled irradiation and specially using direct-write electron beam lithography. For an appropriate choice of vortex density (i.e., of the applied magnetic field) a controllable fraction of the magnetic flux lines penetrating the sample cannot be accommodated in the asymmetric traps, even in the absence of external drive. However, such *excess* vortices still perceive the pin asymmetry through their long-range interaction

with the trapped vortex array. The variety of the dynamical behaviors we observed as a function of drive provides an ideal playground for studying novel spatio-temporal dynamics in a non-equilibrium driven system, including anomalous interstitial dynamics, Stokes' drift, and current inversion.

We focus here on an applied magnetic field slightly above the first matching field because in this dilute limit it is easier to study the dynamics of the moving interstitial vortices interacting with the nearby pinned vortices. The location of these trapped vortices is weakly shifted by the interstitial vortices as they pass very near the trapped vortices. These small shifts of the trapped vortices play an important role inverting the direction of motion of the interstitial vortices.

Fields below the first matching field provide no interstitial vortices. Fields much larger than the first matching field are not useful for rectifying vortex motion. This is easy to see considering an example. If the sample is placed in an externally applied magnetic field which is equal to twice the first matching field there are two vortices for each pinning site. Under usual conditions, the interstitial vortices move back and forth and do not get rectified. Thus, the excess vortices dissipate energy when moving back and forth and their net motion is zero. Maximum rectification is achieved very near the first matching field (experimentally a perfect equal sign is not easy to achieve).

2. Model

In Ref. [11] a lattice of asymmetric double-well pinning centers was generated by means of two interpenetrating square lattices, each one with potential energy wells at each square site and each one with different pinning strengths. These two square pinning lattices are shifted a distance d apart along the y-direction, with d smaller than the lattice constant a_0, here chosen as $a_0 = 1$. Fig. 1(a) shows a schematic top view or x-y view of a small section of a sample with two interpenetrating square arrays of weak and strong pinning sites. Fig. 1(b) shows a small portion of the potential energy landscape over which the vortices move. All N_p pinning centers are modelled by Gaussian potential wells with decay length R_p. The force exerted by the kth pinning site on the ith vortex is [16]

$$\mathbf{F}_k(\mathbf{r}_i) = -F_{p0}^{\gamma} f_0 \left(\frac{\mathbf{r}_i - \mathbf{R}_k}{R_p}\right) \exp\left(-\left|\frac{\mathbf{r}_i - \mathbf{R}_k}{R_p}\right|^2\right), \tag{1}$$

where $\mathbf{r}_i$ represents the location of the ith vortex and $\gamma = w$ ("weak") or s ("strong") characterizes the strength of the kth pinning site located at $\mathbf{R}_k$. The intensity of the individual pinning force is denoted by $F_{p0}^{\gamma} f_0$.

In our simulation, forces (per unit length) are taken in units of $f_0 = \Phi_0^2/8\pi^2\lambda^3$, with Φ_0 the superconducting flux quantum and λ the superconducting penetration depth [17]. Since our pinning strengths F_{p0}^{γ} are unequal, the asymmetry of the lattice can be controlled by d. The driving force acting on the vortices is the Lorentz force $\mathbf{F}_L = \mathbf{J} \times \boldsymbol{\Phi}_0$, where $\mathbf{J}$ is the applied electric current density. Here, an AC current is applied to the sample along the x-direction in the x-y plane, so that the driving Lorentz force $\mathbf{F}_L$ is always parallel to the y-axis. The repulsive vortex-vortex interaction is modelled by

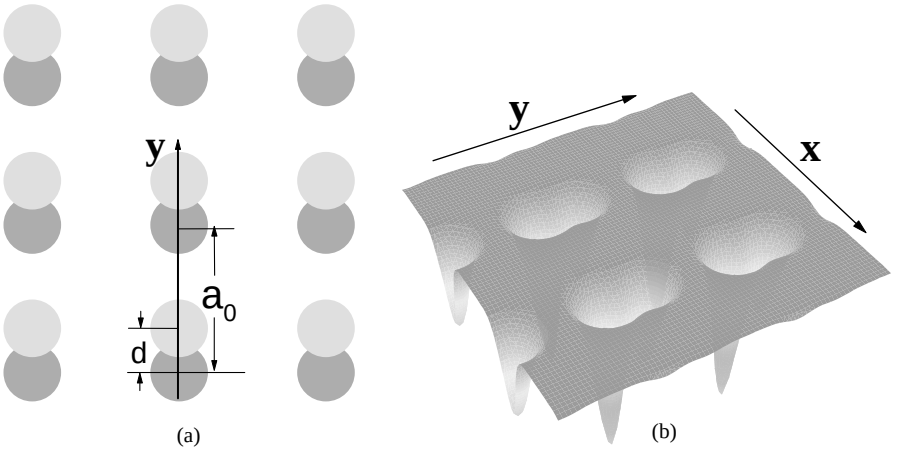

Fig. 1. (a) Schematic top view of a subset of the sample showing two interpenetrating square lattices of pinning sites shifted by $d = 0.2a_0$ along the y-direction. The period a_0 of both the strong pinning lattice (indicated here schematically by darker grey circles) and the weak pinning lattice (lighter grey circles) are the same. Both pinning sites have the same diameter. (b) $3D$ illustration of a small portion of the asymmetric double-well pinning potential energy felt by the vortices in the sample.

a logarithmic potential, $U_{vv} \sim -\ln(r/\lambda)$. Thus, the vortex-vortex repulsive interaction force is

$$\mathbf{F}_{vv}(\mathbf{r}_i) = F_{vv0} f_0 \sum_{j \neq i}^{N_v} \frac{\lambda \hat{\mathbf{r}}_{ij}}{|\mathbf{r}_i - \mathbf{r}_j|} \,, \tag{2}$$

where $\hat{\mathbf{r}}_{ij} = (\mathbf{r}_i - \mathbf{r}_j)/|\mathbf{r}_i - \mathbf{r}_j|$. The intensity of the intervortex interaction force is $F_{vv0} f_0$ and its cut-off length was set to $5a_0$. In the absence of thermal fluctuations [11] the overdamped equation of motion of the ith vortex reads

$$\eta \mathbf{v}_i = \mathbf{F}_L + \mathbf{F}_{vv}(\mathbf{r}_i) + \mathbf{F}_p(\mathbf{r}_i) \,, \tag{3}$$

where η is the viscous damping coefficient (hereafter, $\eta = 1$ for convenience) and $\mathbf{F}_p(\mathbf{r}_i)$ is the total pinning force exerted on the vortex by both sublattices w and s.

The equation of motion for the vortices is solved by taking discrete time steps $\tau_0 = 0.00667$ in a $2D$ square sample containing two interpenetrating arrays of strong and weak pinning sites with periodic boundary conditions in both directions. The initial vortex positions are obtained by annealing, that is, the sample is first exposed to high temperatures and then cooled down to zero temperature. Due to the vortex-vortex repulsion, the low density of excess vortices tend to sit in the channels formed by the columns of trapped vortices. The sample is then subjected to a square-wave alternating current along the x-axis, producing a square-wave Lorentz driving force along the y-axis with amplitude F_L and half period P. The remaining simulation lengths and forces used in the figures here are kept constant: $R_p = 0.13a_0$, $\lambda = 2.6a_0$, $F_{vv0} = 0.1$ and $F^s_{p0} = 0.5$. Other parameter values were also considered, with consistent results. Systematic simulation runs were carried out only for a square sample with size $10a_0 \times 10a_0$, (i.e., with $N_p = 100$

asymmetric pinning centers). We tested samples of different sizes and geometries, as well, coming to the conclusion that our results are insensitive to the sample size, provided that the density of vortices and pinning sites remains unchanged. The number of magnetic vortices N_v is a tunable parameter both in the lab and in the simulations. In experiments N_v is controlled by varying the applied magnetic field H perpendicular to the sample.

A single trapped vortex can be extracted from an isolated composite pinning center by applying an external force with amplitude larger than a characteristic depinning force, namely $F_L > F_m$ when $\mathbf{F}_L \parallel \mathbf{y}$ and $F_L > F_M$ when $\mathbf{F}_L \parallel -\mathbf{y}$. For the pinning parameters adopted throughout the present work, one obtains numerically $F_m \simeq 0.236$ and $F_M \simeq 0.436$, respectively, for the weak and the strong pin stopping force.

3. Vortex mobility: DC drive

To investigate numerically the effect of asymmetric pinning on the vortex motion, we maximized the asymmetry effects [11] by setting the pinning sublattices separation to $d = 0.2a_0$ and the relevant pinning strength ratio to $F^s_{P0}/F^w_{P0} = 2$. We also chose to work immediately above the first matching field H_1; this means that in our simulations the number of vortices N_v is set to be slightly larger than the number of pins N_p (by definition $N_v/N_p = H/H_1$), thus establishing a low density of excess vortices.

The key transport quantity we studied in detail is

$$V_{DC} = \left\langle \frac{1}{N_v} \sum_i^{N_v} v_i \right\rangle_{AC} , \tag{4}$$

where $\langle \cdots \rangle_{AC}$ denotes the *net stationary time-average velocity* over many AC cycles of the driving force (typically 100 or a few hundred cycles). In all our runs stationarity was reached after transient times that were shorter than fifty AC cycles (the transients typically lasted between 20 to 30 cycles).

In order to remove the linear growth component, in Fig. 2 we plot the vortex mobility $\mu_{R,L} = |V_{DC}|/F_L$ versus the amplitude F_L of a DC drive with $\mathbf{F}_L \parallel \mathbf{y}$ (for μ_R) and $\mathbf{F}_L \parallel -\mathbf{y}$ (for μ_L), respectively. In this paper, $\mu_{R,L}$ is a compact way to refer to two quantities: μ_R and μ_L. A step structure is apparent in the vortex mobility versus the amplitude of the driving force, shown in Fig. 2. For large drives, $F_L > F_{m,M}$, all the vortices (core-pinned and interstitial, alike) run in the $\mathbf{F}_L$ direction and the average vortex mobility approaches unity (as it should, since $\eta = 1$). The compact notation $F_L > F_{m,M}$ refers to two inequalities: $F_L > F_m$ and $F_L > F_M$. On decreasing F_L, a first big drop in the mobility curves occurs in the vicinity of F_m for $\mu_R(F_L)$ and of F_M for $\mu_L(F_L)$. In Ref. [11] we showed that the asymptotic branch of both mobility curves can be approximated to $\sqrt{F_L^2 - F_{m,M}^2}$ with $F_L > F_{m,M}$, respectively, as earlier predicted for a Brownian particle in a washboard potential [18,19].

The mobility curves $\mu_{R,L}(F_L)$ for $F_L < F_{m,M}$ are determined by the dynamics of the excess, or interstitial, vortices (just one out of a total of 101 vortices in our sample at $H/H_1 = 1.01$), because the core-pinned vortices are trapped to the pinning lattice.

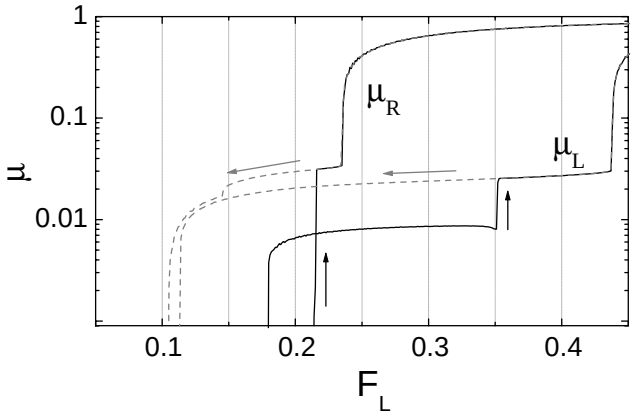

Fig. 2. Vortex mobility curves $\mu_{R,L}$ versus the amplitude F_L of a DC drive at constant magnetic field $H/H_1 = 1.01$, i.e., of a 10×10 vortex array with only one interstitial. The solid curves were obtained starting from an interstitial configuration and ramping up F_L from 0 to 1 by steps of 0.001; the dashed curves were obtained on ramping F_L back down to 0. In the case of μ_R, the Lorentz force $\mathbf{F}_L$ was oriented in the $+\mathbf{y}$ direction, and vice versa for μ_L. The remaining simulation parameters are: $a_0 = 1$, $d = 0.2a_0$, $F^s_{p0} = 0.5$, $F^s_{p0}/F^w_{p0} = 2$ and $\tau_0 = 0.0067$.

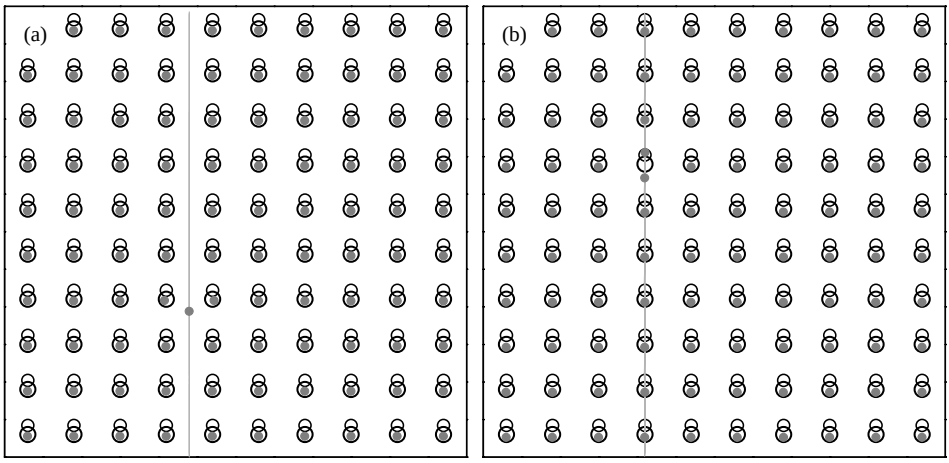

Fig. 3. Vortex trajectories for $H/H_1 = 1.01$ and different intensities of a DC drive oriented in the negative direction (with mobility μ_L shown in Fig. 2): (a) $F_L = 0.3$, interstitial phase; (b) $F_L = 0.4$, discommensuration phase. The remaining simulation parameters are as in Fig. 2.

The $\mu_L(F_L)$ curve in Fig. 2 exhibits two clear-cut steps at $F_L \simeq 0.18$ and 0.35 as F_L is being ramped up from 0 to 1. The latter step clearly indicates a sudden phase transition in the interstitial dynamics. This event is illustrated in Fig. 3: In panel (a) the interstitial runs parallel to $\mathbf{F}_L$ at the center of the channel delimited by two adjacent

(locked) vortex columns; in panel (b) the moving vortex joins a vertical column producing a travelling discrete soliton-like [20] deformation or discommensuration (like in Ref. [17]). A vortex in phase (a) behaves like a proper *interstitial*, while a vortex of phase (b) is rather to be regarded as a lattice *discommensuration*.

The interstitial is subjected to a periodic potential $U_i(y)$ generated by the trapped vortices; such a potential is weaker than the potential $U_p(y)$ responsible for the locking of the vortex lattice, as proved by the inequality $F_m^{(i)} < F_{m,M}$, where $F_m^{(i)} \simeq 0.18$ denotes the first step in the solid curve $\mu_L(F_L)$ of Fig. 2. If we insert the excess vortex of Fig. 3 by hand so as to form a travelling discommensuration and then slowly decrease F_L, the mobility μ_L retraces the entire discommensuration branch (solid line) backwards and then continues it (dashed line) until it drops to zero at $F_M^{(d)} \simeq 0.113$, with no further intermediate step. The inequality $F_M^{(d)} < F_m^{(i)}$ suggests that the discommensuration phase is stable and at low drive amplitudes is more mobile than the interstitial phase.

The analysis of the $\mu_R(F_L)$ curve is simpler. When starting with an interstitial configuration and ramping F_L up, we detected a sudden jump in $\mu_R(F_L)$ from a completely locked phase, where not even the interstitial vortex moved, to a "travelling discommensuration phase" at around $F_L \simeq 0.215$. On ramping F_L down to zero, the discommensuration comes to a complete stop for $F_m^{(d)} \simeq 0.105$. For the simulation parameters of Fig. 2, a stable interstitial phase never shows up for $\mathbf{F}_L \parallel \mathbf{y}$.

The mobility curves in Fig. 2 are an (almost linear) superposition of three distinct depinning processes involving, respectively: (1) the trapped vortex lattice; (2) the discommensurations; (3) the (proper) interstitials. All three classes of objects move on quasi-one dimensional periodic asymmetric substrates in the y-direction. In particular, discommensurations are well represented by extended quasi-particles diffusing on periodic $1D$ potentials [20]. Here, as both $F_m^{(d)} < F_M^{(d)}$ and $F_m < F_M$, the effective ratchet potentials for the vortex lattice and the discommensurations are expected to show the same polarity.

Finally, let us now consider the height of the mobility steps in Fig. 2. Here, the normalization in the definition (4) of V_{DC} plays an important role. The asymptotic branch of both μ_R and μ_L approaches unity, when F_L grows, because after depinning all $N_v = 101$ vortices of the sample move in the $\mathbf{F}_L$ direction with speed close to F_L. On the contrary, the height of the interstitial step of μ_L (for $F_L \simeq 0.18$ for μ_L in Fig. 2) is about one hundredth the asymptotic mobility value ($\mu \to 1$), as to be expected in the presence of one mobile interstitial among 101 vortices. However, the discommensuration step ($F_L \simeq 0.35$ for μ_L in Fig. 2), is about three times as large as the interstitial one, thus implying that the effective mobility of an isolated discommensuration in our simulation is a about three times larger than the mobility of an interstitial vortex.

4. Rectification mechanisms for AC driven vortices

So far we have analyzed the response of the vortex system to a DC driving force, induced by a DC applied current. We are now in a position to study the vortex response to a square-wave AC drive—applied along the y-axis, with amplitude F_L and half period P. The curve V_{DC} versus P for an amplitude value in the range (F_m, F_M) and

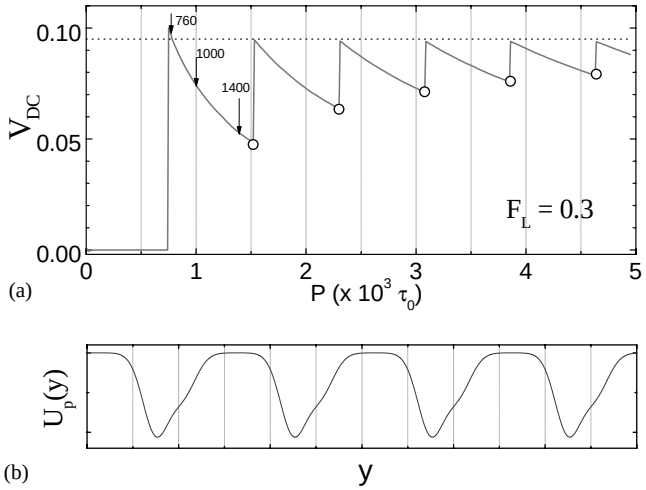

Fig. 4. (a) Average net vortex velocity V_{DC} versus the drive half-period P at constant magnetic field $H/H_1 = 1.01$ and drive amplitude $F_L = 0.3$. Snapshots of the vortex trajectories for the P values indicated by the vertical arrows are displayed in Fig. 6; (b) The corresponding asymmetric pinning potential $U_p(y)$ experienced by a vortex moving along a vertical column of pinning centers. The remaining simulation parameters are as in Fig. 2. In panel (a) the horizontal dotted line is V_M and the open circles represent $V_m(n)$ for $n = 1$ through 5.

$H/H_1 = 1.01$ is displayed in Fig. 4(a). Notice that the collective motion of the vortex array gets rectified in the *positive* y-direction through a sequence of depinning (for $\mathbf{F}_L \| \mathbf{y}$, positive half cycle) and re-pinning events (for $\mathbf{F}_L \| -\mathbf{y}$, negative half cycle). On increasing the drive half-period from $P = 0$ up to $5000\tau_0$ with small step $\Delta P = 10\tau_0$, the rectified vortex response V_{DC} develops a sharp sawtooth structure, that tapers out at asymptotically large P values.

When P is sufficiently small, the driven vortices travel a distance smaller than the minimum interpin distance $a_0 - d - 2R_p$ during a positive half period P; afterwards, the vortices are driven back to the original pinning center during the subsequent negative half period. This results in a zero DC response of the trapped vortex lattice (on the linear scale of Fig. 4(a), interstitial transport at $H/H_1 = 1.01$ is negligible).

When the period of the driving force exceeds a threshold value P_c, which depends on F_L, the vortices move from one pinning site to another one nearby during a half period and the system acts as a vortex rectifier or a *collective* "*stepmotor*" of flux quanta. In Ref. [11] the threshold half period is approximated to $P_c = a_0/\langle u \rangle$, where $\langle u \rangle = \kappa(F_L)F_L \simeq F_L(1 - \delta_p F_m/F_L)$ with $\delta_p = 2R_p + d$ is an estimate of the vortex velocity in the periodic substrate potential $U_p(y)$ plotted in Fig. 4(b).

The curve $V_{DC}(P)$ versus P shows a sequence of peaks of the same height $V_{DC} = V_M$. These peaks correspond to $P = nP_c + 0$, i.e., to the driving condition when a single vortex can advance by n lattice constants a_0 in the y-direction during a positive half cycle. The peak velocity is therefore $V_M = na_0/2nP_c = \kappa(F_L)F_L/2$. The minima $V_m(n)$ of the curve V_{DC} versus P occur at $P = nP_c - 0$, as the vortex drifts a distance na_0 in

a positive half period of duration $(n+1)P_c$; accordingly,

$$V_m(n) = V_M\, n/(n+1)\,,$$

with $n = 1, 2, 3, \ldots$. Both predictions for V_M and $V_m(n)$ are displayed in Fig. 4(a). Note the *positive* polarity of $U_p(y)$ under periodic tilting (as in the AC, tilted, or rocked ratchet [21]).

Let us focus now on the interstitial dynamics relative to the trapped vortex array; the latter can be either locked for $F_L < F_m$, or advance by means of the stepmotor mechanism just described for $F_m < F_L < F_M$, or run back and forth (with a net drift in the positive y-direction) for $F_L > F_M$. We distinguish two different operating conditions below and above threshold. These will be separately considered below.

5. Sub-threshold AC dynamics

For $F_M^{(i)} < F_L < F_m$, the one excess vortex at $H/H_1 = 1.01$ undergoes rectification under the influence of the external AC drive. In Fig. 5(a) we display two $V_{DC}(P)$ curves, for $F_L = 0.2$ and 0.225. The net velocity curve for $F_L = 0.2$ is *negative* over the entire P domain we simulated and exhibits a sawtooth structure resembling that shown in Fig. 4(a). Once again, the onset jump at $P_c \simeq 1150\tau_0$ coincides with the distance between two adjacent V_{DC} peaks at higher P values. Moreover, the approximate formula for P_c as a function of F_L proposed in Ref. [11] (see above) appears to hold good in this sub-threshold regime, too.

The net velocity curve for $F_L = 0.225$ follows a similar pattern up to $P_c \simeq 2850\tau_0$, where it suddenly *turns positive* and much less ragged. To clarify the nature of such

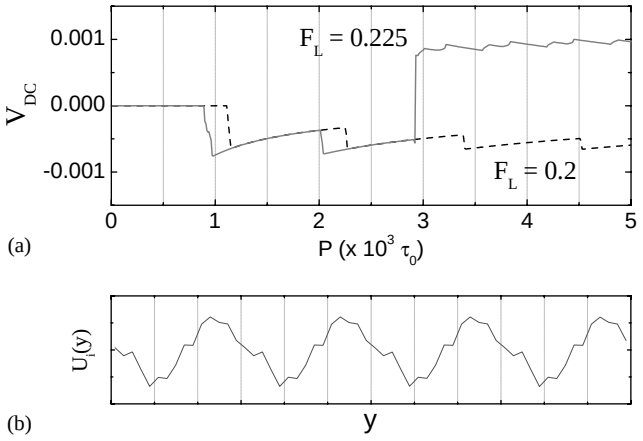

Fig. 5. (a) Average net vortex velocity V_{DC} versus the drive half-period P at constant magnetic field $H/H_1 = 1.01$ and different drive amplitudes $F_L = 0.2$ (dashed curve) and 0.225 (solid curve); (b) The corresponding asymmetric pinning potential $U_i(y)$ experienced by an interstitial moving along the channel formed by two adjacent columns of trapped vortices. The irregularities in the curve $U_i(y)$ are due to the finite cut-off length of the force F_{vv}. The remaining simulation parameters are as in Fig. 2.

an abrupt change, we took snapshots of the vortex assembly before and after current reversal and concluded that the negative branch of the curve (and the entire curve for $F_L = 0.2$) describes the time evolution of a proper interstitial, while the positive branch corresponds to the rectification of a discommensuration.

The single particle argument developed for the collective vortex motion at large drives, $F_L > F_m$, can be readily adjusted to describe an interstitial moving on the ratchet potential $U_i(y)$ of Fig. 5(b). Our numerical characterization of $U_i(y)$ reveals an asymmetric periodic interstitial potential with cell unit a_0 and *reversed* polarity with respect to the lattice ratchet potential $U_p(y)$. The negative polarity of $U_i(y)$ is a consequence of the asymmetric shape of the pinning centers in Fig. 1: A trapped vortex can be pushed more easily from the weak to the strong pinning sub-unit than vice versa; therefore, the driven interstitial encounters a slightly softer resistance to its motion in that (negative) direction than in the opposite (positive) direction. Hence, its negative rectified velocity V_{DC}.

We already anticipated that the discommensuration effective potential must have the same positive polarity (and periodicity) as $U_p(y)$. This fact was proven for an asymmetric Frenkel-Kontorova model in Ref. [22]. A simple argument goes as follows: an excess vortex moves along a column continuously pushing out of a trap a nearby trapped vortex; on advancing in the positive direction, the discommensurate vortex displaces the pinned vortex immediately ahead by pushing it out of its trap through the weaker site; vice versa to move in the negative direction, the discommensuration has to displace a nearby trapped vortex through the stronger site. The corresponding stopping forces $F_m^{(d)}$ and $F_M^{(d)}$ differ enough from one another to ratchet the discommensuration in the positive direction.

6. Supra-threshold AC dynamics

For $F_L > F_m$ the interstitial flow becomes negligible in comparison with the collective dynamics of the vortex array. Still, interstitial vortices exhibit a complicated, intriguing behavior. Here, we limit our analysis to the first sawtooth of the $V_{DC}(P)$ in Fig. 4(a), where the three distinct dynamical phases of Fig. 6 were resolved.

Panel (a) in Fig. 6 is representative of the interstitial dynamics with drive half-period in the domain $(750\tau_0, 790\tau_0)$. The net interstitial velocity is *positive*, as the interstitial is dragged along by the trapped vortex lattice moving in unison. This is an instance of a mechanism known as Stokes' drift [23]. The occurrence of such an effect requires a high degree of synchronization between the interstitial and the vortex lattice oscillations, which can only be attained in the vicinity of P_c. The positive Stokes' drift of the interstitials contributes an additional term to the average velocity of the vortex array for $P \sim P_c$. This explains, for instance, the tiny bump detectable right at the tip of the first peak of the $V_{DC}(P)$ curve in Fig. 4(a).

Panel (b) shows the effect of increasing P in the interval $(800\tau_0, 1240\tau_0)$. The interstitial moves more freely than the trapped vortices; therefore, over longer drive half-periods no synchronization is possible; moreover, the interstitial becomes less sensitive to the pinning asymmetry, as the initially trapped vortices spend a substantial

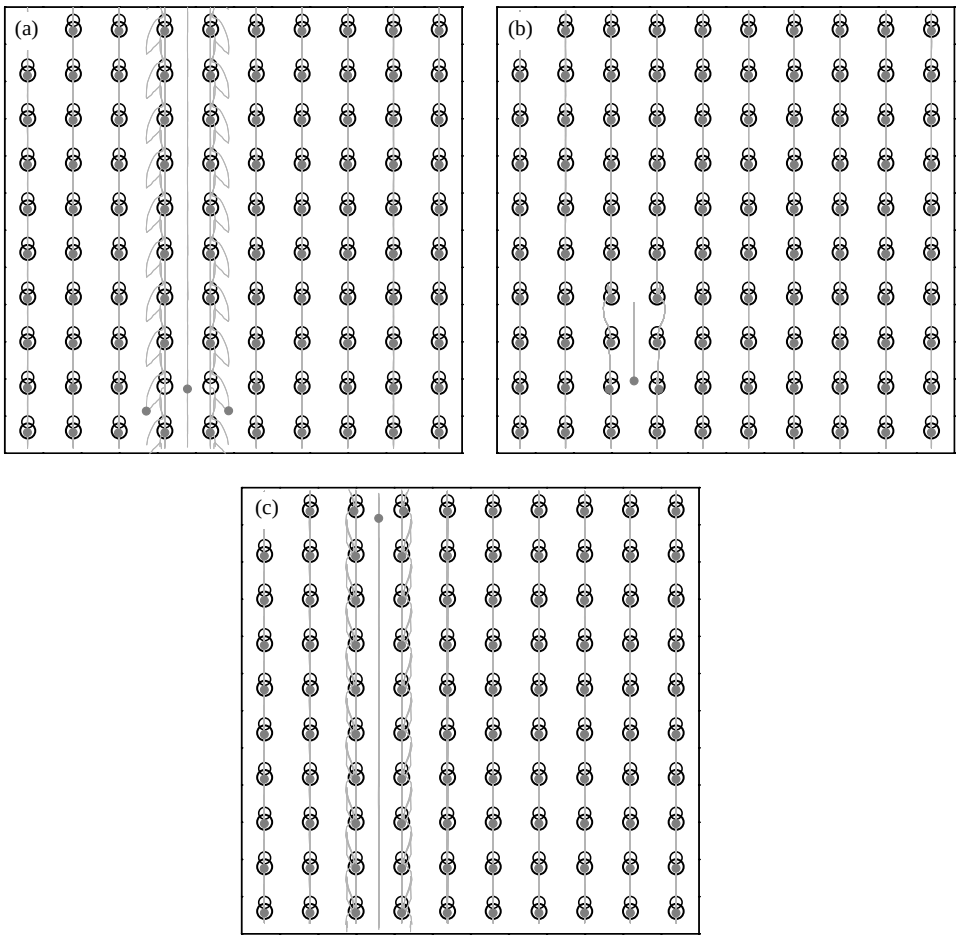

Fig. 6. Interstitial trajectories for $H/H_1 = 1.01$, $F_L = 0.3$ and different half-periods of the driving force as indicated in Fig. 4: (a) $P = 760\tau_0$, *positive net interstitial velocity* (*Stokes' drift*); (b) $P = 1000\tau_0$, *interstitial oscillations*, *no net drift*; (c) $P = 1400\tau_0$ *negative net interstitial velocity* (*ratchet effect*). The remaining simulation parameters are as in Fig. 2.

fraction of their time in the interpin region. As a result the interstitial starts oscillating back and forth with *no net drift* in either direction.

Panel (c) illustrates the onset of an interstitial rectification mechanism in the presence of collective vortex oscillations. This may require longer drive half-periods than in the sub-threshold case, but it eventually does happen. For AC half periods corresponding to the last portion of the first V_{DC} sawtooth, $(1250\tau_0, 1490\tau_0)$, the interstitial succeeds in covering a distance equal to two pinning lattice constants, while the slower trapped vortices do not; the rectification mechanism sets on and the interstitial acquires a *negative* net velocity.

Finally, for $P > 1500\tau_0$, that is starting with the second V_{DC} sawtooth, the interstitial disappears, replaced by a discommensuration. We checked that for $P=2000\tau_0$ at $F_L=0.3$ the average net velocity $\bar{v}_d \simeq 0.060$ of a single vortex in a discommensurate column ($10a_0$ long and subject to periodic boundary conditions), is significantly smaller than the average net velocity $\bar{v} \simeq 0.075$ of a vortex in a regular column. The explanation of this behavior is qualitatively simple. During a positive half cycle all columns, regular and discommensurate, alike, move in the positive direction in unison since $F_L > F_m$; during a negative half cycle regular columns get locked immediately (here, $F_L < F_M$), whereas the discommensurations can travel in the negative direction as long as F_L is larger than $F_M^{(d)}$ (which we know being smaller than F_m). The incomplete re-pinning of the vortices forming a discommensuration during a negative drive half cycle, degrades their average net velocity in the positive direction. This interpretation of the discommensuration dynamics in the supra-threshold regime can be checked quantitatively, too, with the aid of Fig. 2.

7. Conclusions

In summary, we have studied the interstitial dynamics in superconductors with regular arrays of asymmetric pinning centers subjected to an AC "square wave" electrical current. Interstitials can be found in two stable dynamical phases depending on the drive amplitude and period: proper interstitials diffusing in vertical channels parallel to the applied drive, and discommensurations moving like finite density pulses along vertical trapped vortex columns. At low amplitudes, AC driven transport of interstitials and discommensurations show opposite ratchet polarity. At larger drive amplitudes, discommensurations and the vortex lattice drift in the same direction under the action of an external periodic force; exceptionally, interstitials may be dragged along by the vortex lattice when certain synchronization conditions are fulfilled. These effects and other related ratchet effects [24] could be visualized using Lorentz microscopy [25]. It is important to emphasize that our results also apply to arrays of Josephson junctions, colloidal systems, Wigner crystals and any system with repelling movable objects that can be pinned by a lattice of traps.

Acknowledgements

We acknowledge support from the Frontier Research System and the International Cooperation Office of RIKEN, Japan, and the US National Science Foundation, via grant No. EIA-0130383. The authors thank the Advanced Computing Center at RIKEN for providing access to their Fujitsu VPP700 supercomputer.

References

[1] H. Linke (Ed.), Ratchets and Brownian Motors: Basics, Experiments and Applications, Special Issue of Appl. Phys. A 75 (2) (2002).

[2] P. Hänggi, P. Reimann, Phys. World 12 (1999) 21.
[3] P. Reimann, Phys. Rep. 361 (2002) 57.
[4] R.D. Astumian, P. Hänggi, Phys. Today 55 (11) (2002) 33.
[5] F. Jülicher, A. Ajdari, J. Prost, Rev. Mod. Phys. 69 (1997) 1269.
[6] C.R. Doering, Physica A 254 (1998) 1;
C.R. Doering, L.A. Dontcheva, M.M. Klosek, Chaos 8 (1998) 643;
C.R. Doering, W. Horsthemke, J. Riordan, Phys. Rev. Lett. 72 (1994) 2984;
I. Derènyi, T. Vicsek, Phys. Rev. Lett. 75 (1995) 374.
[7] F. Nori, Science 278 (1996) 1373;
C.J. Olson, C. Reichhardt, F. Nori, Phys. Rev. Lett. 80 (1998) 2197;
C.J. Olson, C. Reichhardt, F. Nori, Phys. Rev. Lett. 81 (1998) 3757;
C. Reichhardt, F. Nori, Phys. Rev. Lett. 82 (1999) 414;
O. Pla, F. Nori, Phys. Rev. Lett. 67 (1991) 919;
R. Richardson, S.D. Peacor, C. Uher, F. Nori, Phys. Rev. Lett. 67 (1991) 3856;
R. Richardson, O. Pla, F. Nori, Phys. Rev. Lett. 72 (1994) 1268;
S. Field, J. Witt, F. Nori, X. Ling, Phys. Rev. Lett. 74 (1995) 1208;
C. Reichhardt, C.J. Olson, J. Groth, S. Field, F. Nori, Phys. Rev. B 52 (1995) 10 441;
C. Reichhardt, C.J. Olson, J. Groth, S. Field, F. Nori, Phys. Rev. B 53 (1996) 8898.
[8] H. Weinstock (Ed.), Applications of Superconductivity, Kluwer, Dordrecht, 1999;
H. Weinstock (Ed.), SQUID Sensors, Kluwer, Dordrecht, 1996;
H. Weinstock (Ed.), New Superconducting Electronics, Kluwer, Dordrecht, 1993;
H. Weinstock, M. Nisenoff (Eds.), Superconducting Electronics, Springer, Heidelberg, 1989;
H. Weinstock, Physica C 209 (1993) 269;
H. Weinstock, IEEE Trans. Mag. 27 (1991) 3231.
[9] J.F. Wambaugh, C. Reichhardt, C.J. Olson, F. Marchesoni, F. Nori, Phys. Rev. Lett. 83 (1999) 5106.
[10] C.J. Olson, C. Reichhardt, B. Janko, F. Nori, Phys. Rev. Lett. 87 (2001) 17 702;
W. Kwok, et al., unpublished experimental results.
[11] B.Y. Zhu, F. Marchesoni, V.V. Moshchalkov, F. Nori, 2003, submitted.
[12] B.Y. Zhu, F. Marchesoni, F. Nori, Physica E 18 (2003) 318–319;
B.Y. Zhu, L. Van Look, V.V. Moshchalkov, F. Marchesoni, F. Nori, Physica E 18 (2003) 322–324.
[13] J. Groth, C. Reichhardt, C.J. Olson, S.B. Field, F. Nori, Phys. Rev. Lett. 77 (1996) 3625.
[14] C.S. Lee, B. Janko, I. Derenyi, A.L. Barabasi, Nature 400 (1999) 337.
[15] S. Savelev, F. Nori, Nat. Mater. 1 (2002) 179.
[16] B.Y. Zhu, L. Van Look, V.V. Moshchalkov, B.R. Zhao, Z.X. Zhao, Phys. Rev. B 64 (2001) 012 504.
[17] C. Reichhardt, C.J. Olson, F. Nori, Phys. Rev. Lett. 78 (1997) 2648;
C. Reichhardt, C.J. Olson, F. Nori, Phys. Rev. B 58 (1998) 6534.
[18] G. Costantini, F. Marchesoni, Europhys. Lett. 48 (1999) 491.
[19] H. Risken, The Fokker-Planck Equation, Springer, Berlin, 1984 (Chapter 11).
[20] C. Cattuto, G. Costantini, T. Guidi, F. Marchesoni, Phys. Rev. B 63 (2001) 094 308.
[21] R. Bartussek, P. Hänggi, J.G. Kissner, Europhys. Lett. 28 (1994) 459;
F. Marchesoni, Phys. Lett. A 237 (1998) 123;
M. Borromeo, G. Costantini, F. Marchesoni, Phys. Rev. E 65 (2002) 041 110.
[22] F. Marchesoni, Phys. Rev. Lett. 77 (1996) 2364;
G. Costantini, F. Marchesoni, Phys. Rev. Lett. 87 (2001) 114 102.
[23] M. Borromeo, F. Marchesoni, Phys. Rev. B 65 (2002) 184 101;
M. Borromeo, F. Marchesoni, Phys. Lett. A 249 (1998) 199;
C. Van den Broeck, Europhys. Lett. 46 (1999) 1;
K.M. Jansons, G.D. Lythe, Phys. Rev. Lett. 81 (1998) 3136.
[24] R. Bartussek, P. Hänggi, J.G. Kissner, Europhys. Lett. 28 (1994) 459;
R. Bartussek, P. Reimann, P. Hänggi, Phys. Rev. Lett. 76 (1996) 1166;
P. Jung, J.G. Kissner, P. Hänggi, Phys. Rev. Lett. 76 (1996) 3436;
P. Reimann, C. Van den Broek, H. Linke, P. Hänggi, J.M. Rubi, A. Perez, Phys. Rev. Lett. 87 (2001) 010 602;
R. Eichhorn, P. Reimann, P. Hänggi, Phys. Rev. Lett. 88 (2002) 190 601;

J. Lehmann, S. Kohler, P. Hänggi, A. Nitzan, Phys. Rev. Lett. 88 (2002) 228 305;
D. Reguera, P. Reimann, P. Hänggi, J.M. Rubi, Europhys. Lett. 57 (2002) 644;
P. Reimann P. Hänggi, Appl. Phys. A 75 (2002) 169.
[25] A. Tonomura, Physica B 280 (2000) 227;
A. Tonomura, Int. J. Mod. Phys. 15 (2000) 3427;
A. Tonomura, Micron 30 (1999) 479;
A. Tonomura, H. Kasai, O. Kamimura, T. Matsuda, K. Harada, J. Shimoyama, K. Kishio, K. Kitazawa, Nature 397 (1999) 308;
C.H. Sow, K. Harada, A. Tonomura, G. Crabtree, D.G. Grier, Phys. Rev. Lett. 60 (1998) 2693;
N. Osakabe, H. Kasai, T. Kodama, A. Tonomura, Phys. Rev. Lett. 78 (1997) 1711;
K. Harada, O. Kamimura, H. Kasai, T. Matsuda, A. Tonomura, V.V. Moshchalkov, Science 274 (1996) 1167;
T. Matsuda, K. Harada, H. Kasai, O. Kamimura, A. Tonomura, Science 271 (1996) 1393.